Vol. 14 • No. 12 • March 25 • 2026
www.advopticalmat.de

ADVANCED OPTICAL MATERIALS

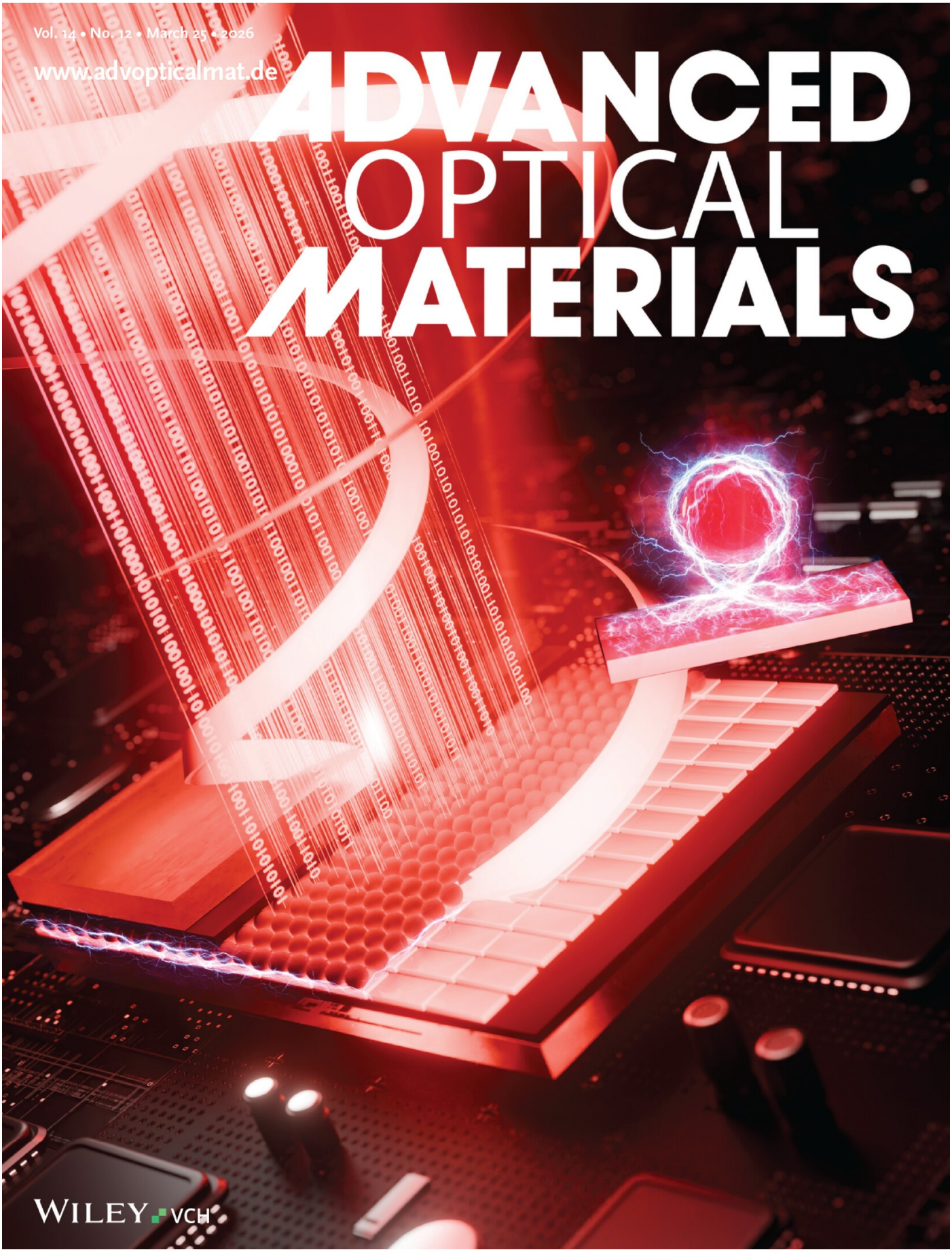

WILEY VCH

Check for updates

ADVANCED OPTICAL MATERIALS
www.advopticalmat.de

Solution-Processed Spin-Polarized Light-Emitting Diodes of Colloidal Quantum Wells and Magnetic Nanoparticles

Savas Delikanli, Arinjoy Bhattacharya, Betul Canimkurbey, Chang Huai, Amani Almutairi, Arman Najafi, Hilal Korkut, Farzan Shabani, Furkan Isik, James Pientka, Ibrahim Sarpkaya, Hao Zeng, Richard D. Schaller, Athos Petrou,* and Hilmi Volkan Demir**

Electrical injection of spin-polarized carriers into semiconductors enables circularly-polarized emission from spin-polarized light-emitting diodes (spin-LEDs). The incredible level of tunability of magnetic and electronic properties in colloidal nanocrystals offers unprecedented opportunities for the modulation of polarization of light in solution-processed spin-LEDs based on magnetic nanoparticles unlike epitaxially grown spin-LEDs restricted by a very limited range of materials for their exploitation, and solution-processed spin-LEDs based on chiral molecules, which do not allow the modulation of polarization in general. Here, it is shown that electrical injection of spin-polarized electrons from magnetic Fe_3O_4 nanoparticles into CdSe/CdZnS core/shell colloidal quantum wells (CQWs) in solution-processed LEDs that allows for polarization modulation of electroluminescence. In this structure, a monolayer of face-down oriented CQWs is deposited as an active layer to avoid polarization losses due to the hopping of the electrons between the CQWs before the radiative recombination process. In this solution-processed spin-LED, the circular polarization reaches 4.5% at 3 K and survives up to 100 K. A net circular polarization is observed at zero magnetic field up to 100 K because of the remnant magnetization of the Fe_3O_4 nanoparticles. This new colloidal spin-LED architecture presents significant prospects for future solution-processed advanced opto-spintronic devices.

1. Introduction

The modulation of spin angular momentum of carriers enables novel functionalities in semiconductors, which can be exploited in optoelectronic applications.[1] Because of the practical importance of the manipulation of carrier spins, the field of spintronics has been growing rapidly since the discovery of giant magnetoresistance. This progress has led to the development of various spintronic devices, including spin-polarized light-emitting diodes (spin-LEDs).[2–5] In a spin-LED, spin-polarized carriers are electrically injected into a semiconductor through a spin injector to emit circularly polarized light, which can be used for quantum information applications, chiral synthesis, and modulation of ultrafast magnetization.[4,6–10] The degree of circularly polarized electroluminescence (EL) of a spin-LED is determined by the spin-injection efficiency, spin relaxation lifetime and recombination lifetime of the carriers.[4,6,11,12] The correlation

S. Delikanli, B. Canimkurbey, H. Korkut, F. Shabani, F. Isik, I. Sarpkaya, H. V. Demir
Department of Electrical and Electronics Engineering
Department of Physics
UNAM-Institute of Materials Science and Nanotechnology and the National Nanotechnology Research Center
Bilkent University
Ankara 06800, Turkey
E-mail: savasdel@bilkent.edu.tr; volkan@stanfordalumni.org

The ORCID identification number(s) for the author(s) of this article can be found under https://doi.org/10.1002/adom.202502254

© 2025 The Author(s). Advanced Optical Materials published by Wiley-VCH GmbH. This is an open access article under the terms of the Creative Commons Attribution License, which permits use, distribution and reproduction in any medium, provided the original work is properly cited.

DOI: 10.1002/adom.202502254

S. Delikanli, H. V. Demir
Luminous! Centre of Excellence for Semiconductor Lighting and Displays
School of Electrical and Electronic Engineering
School of Physical and Mathematical Sciences
School of Materials Science and Engineering
Nanyang Technological University
Singapore 639798, Singapore

A. Bhattacharya, C. Huai, A. Almutairi, A. Najafi, H. Zeng, A. Petrou
Department of Physics
University at Buffalo
State University of New York
Buffalo, NY 14303, USA
E-mail: petrou@buffalo.edu

B. Canimkurbey
Department of Physics
Polatli Faculty of Arts and Sciences
Ankara Hacı Bayram Veli University
Ankara 06900, Turkey

between the spin angular momentum and the optical polarization makes spin-LEDs an excellent platform for investigating and understanding the fundamentals of spin phenomena in semiconductors, which in turn will assist further development of advanced spintronic devices.

Spin-LEDs have been fabricated using epitaxial growth techniques including molecular beam epitaxy (MBE) for a few decades and, in these spin-LEDs, spin polarized carriers are injected through employing either a ferromagnetic or diluted magnetic semiconductor (DMS) layer as a spin injector.[5] In these epitaxially grown spin-LEDs, typically a ferromagnetic Fe layer or a DMS layer made of either ZnMnSe or CdMnTe were employed for spin injection, while GaAs/AlGaAs quantum wells (QW) were used as the emissive layer.[5,12–15] Recently, spin injection into Si was also demonstrated using an Fe contact via MBE.[3] Very limited range of available materials for spin-injection and emissive layers in these epitaxially grown spin-LEDs has hindered the full exploitation of their potential thus far. Very recently a spin-LED based on solution-processed materials has been demonstrated using a chiral metal-halide perovskite layer with no polarization modulation.[11] This previous work relies on chiral-induced spin selectivity as the spin aligner. This solution-processed spin-LED based on a metal-halide perovskite chiral layer, however, undesirably is not capable of the modulating of the optical polarization, which is an indispensable key parameter in applications such as quantum information, encoding, and modulation of ultrafast magnetization.

Solution-processed LEDs based on magnetic nanoparticles provide valuable opportunities to overcome the limitations of these previously fabricated spin-LEDs with numerous available materials for spin-injection and emissive layers. Colloidal magnetic nanoparticles with highly controlled size, shape and composition,[16–18] and ease of formation of multicomponent heterostructures,[19,20] allow for customizing their magnetic properties for different applications, such as information storage,[21] nanocomposite magnets,[22] and bio-applications such as remote stimulation of neurons,[23] magnetic resonance imaging[24] and tumor treatment.[25,26] In particular, magnetite (Fe_3O_4) nanoparticle arrays have demonstrated exceptionally high carrier spin polarization and sizable magnetoresistance at room-temperature,[27] making them a promising candidate as a spin injector in spin-LEDs.

A. Almutairi
Department of Physics
College of Science
Qassim University
Buraydah 52571, Saudi Arabia
J. Pientka
Department of Physics
St. Bonaventure University
St. Bonaventure, NY 14778, USA
R. D. Schaller
Department of Chemistry and the International Institute for Nanotechnology
Northwestern University
Evanston, Illinois 60208, USA
R. D. Schaller
Center for Nanoscale Materials
Argonne National Laboratory
Argonne, Illinois 60439, USA

Among the solution-processed nanocrystals, colloidal QWs (CQWs) are an exceptional class of materials as an emissive layer for solution-processed spin-LEDs, thanks to their highly tunable emission in the visible range, narrow emission linewidth, high photoluminescence quantum efficiency, and short recombination lifetimes (τr) at both room and low temperatures. τr of CQWs is at least an order of magnitude smaller than that of QDs emitting in a similar spectral regime,[28,29] due to the giant oscillator strength and much smaller dark-bright exciton splitting.[29] Additionally, CQWs exhibit non-degenerate heavy and light hole states similar to their epitaxial counterparts.[4] In the context of spin-LEDs, both a short τr and non-degenerate hole states are beneficial for achieving a high degree of circularly polarized emission,[29,30] since the circular polarization is determined by the ratio between radiative recombination and spin lifetimes, and a degenerate hole state would halve the achievable polarization due to the contribution from the light hole state with opposite polarization.[4,14]

The advantages of both CQWs and magnetic nanoparticles raise the tantalizing opportunity for realizing all solution-processed spin-LEDs by combining the two types of materials, in which QWs are used as the emitter and the magnetic nanoparticle layer are used as the spin injector. Colloidal semiconductor and magnetic nanostructures with well-controlled size and shape can be dispersed in solution, which allows for all-solution-processed spin-LEDs using cost-effective techniques such as spin-coating and self-assembly. More importantly, with the flexibility of choosing a variety of QW and magnetic materials, these solution-processed spin-LEDs may help to overcome the limitations of previously fabricated spin-LEDs.

In this work, we report the first attempt to fabricate all-solution-processed spin LEDs based on colloidal Fe_3O_4 nanoparticles and CdSe/CdZnS core/shell CQWs. With these devices, we demonstrate electrical injection of spin-polarized carriers from Fe_3O_4 nanoparticle layer into the CdSe/CdZnS CQWs, realizing circularly polarized emission that can be modulated by a magnetic field. We achieved a circular polarization of 4.5% at 3 K. The circular polarization persists up to 100 K. In addition, we demonstrated a net circular polarization in the absence of an externally applied magnetic field up to 100 K, owing to the remnant magnetization of Fe_3O_4 nanoparticles. We further obtained the temperature-dependent spin relaxation lifetimes using polarized transient absorption (TA) spectroscopy and PL lifetime using a time-resolved photoluminescence (TRPL) spectroscopy. The spin lifetime in CdSe/CdZnS core/shell CQWs reaches 1.3 ns at 3 K and decreases as the temperature is raised and is attributed to the D'yakanov–Perel spin relaxation mechanism. The calculated spin injection efficiency is ≈35% in our spin-LED, which is similar to spin injection efficiencies from Fe contacts to GaAs QWs.[4]

2. Results and Discussion

In this study, we employed chemically synthesized CdSe/CdZnS core/shell CQWs[31] and Fe_3O_4 magnetic nanoparticles[17] in our solution-processed spin-LED structure. The size of the synthesized Fe_3O_4 magnetic nanoparticles is ≈10 nm, as can be seen in the transmission electron microscopy (TEM) image in **Figure 1a**. Details of the synthesis of Fe_3O_4 magnetic nanoparticles are provided in the Supporting Information. Fe_3O_4 exhibits

© 2025 The Author(s). Advanced Optical Materials published by Wiley-VCH GmbH

21951071, 2026, 12, Downloaded from https://advanced.onlinelibrary.wiley.com/doi/10.1002/adom.202502254 by Hilmi Demir - Bilkent University , Wiley Online Library on [29/03/2026]. See the Terms and Conditions (https://onlinelibrary.wiley.com/terms-and-conditions) on Wiley Online Library for rules of use; OA articles are governed by the applicable Creative Commons License

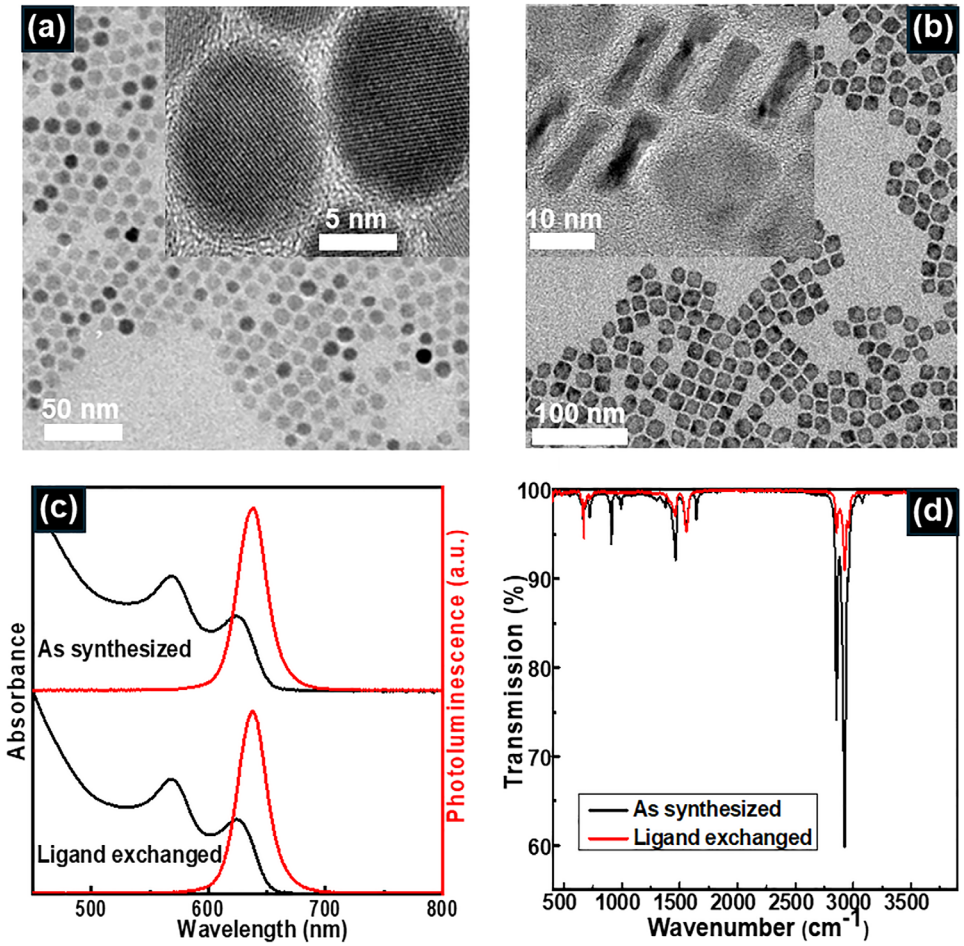

Figure 1. Structural and optical characterizations of the colloidal Fe_3O_4 magnetic nanoparticles and CdSe/CdZnS core/shell CQWs. TEM images of a) Fe_3O_4 magnetic nanoparticles and b) CdSe/CdZnS core/shell CQWs. The insets of (a) and (b) show the high-resolution TEM images of the nanoparticles. c) Absorption and PL profiles of CQWs before and after the ligand exchange. d) FTIR spectrum showing the successful ligand exchange.

a Curie temperature of ≈570 °C, which makes it a promising candidate for realizing spin injection at room-temperature. In addition, it has also been theoretically predicted to be a half-metal with 100% spin polarization, which means only the minority spin (spin down) states are occupied, while the Fermi energy falls in the gap of the majority spin (spin up) DOS. While true half-metallicity is hardly achieved at finite temperatures and with spin–orbit coupling (which mixes the spin up and spin down states), it could still be a material providing a high carrier spin polarization. Indeed, we have shown earlier that Fe_3O_4 nanoparticles exhibit impressive transport spin polarization.[27] Magnetoresistance (MR) of 35% was achieved at 60 K in Fe_3O_4 nanoparticle tunnel junction arrays with random orientation, which translates to ≈70% spin polarization.[27] A material with a high carrier spin polarization is a prerequisite for efficient spin injection in spin-LEDs.

CdSe/CdZnS core/shell CQWs used in this work was synthesized via the seed-mediated growth method.[31] To obtain CdSe/CdZnS core/shell CQWs, 4 ML CdSe CQWs were used as seeds. These core CQWs possess a narrow green emission at 511 nm with a full-width-at-half-maximum (FWHM) of 10 nm (shown in Figure S1, Supporting Information), owing to their atomically flat surfaces and uniform thickness. A wide-gap CdZnS shell layer was grown around the seed CdSe CQWs to suppress nonradiative recombination via surface traps and allow for longer spin-relaxation lifetimes. Details of the synthesis procedures are given in the Supporting Information. The lateral size of the CdSe/CdZnS core/shell CQWs is ≈15 nm as can be seen in the TEM image shown in Figure 1b. The surface of the as-synthesized CdSe/CdZnS core/shell CQWs is passivated with oleic acid (OA) and oleylamine (OLA). These CdSe/CdZnS core/shell CQWs emit at 637 nm with a FWHM of 28 nm, with contributions from only the heavy hole states, as presented in Figure 1c. The PL quantum yield (PLQY) reaches close to ≈90%, which can be attributed to the effective passivation with the wide gap shell and organic ligands. In addition, CdZnS shell enhances the spin relaxation lifetimes strongly as demonstrated earlier,[32] which is necessary for achieving circularly polarized EL emission. Hence, the CdZnS shell is expected to not only enhance the efficiency of the LED device but also boost the EL circular polarization. In addition, the spin-relaxation lifetime of CdSe/CdZnS core/shell CQWs is almost an order magnitude longer than that of CdSe/ZnS core/shell CQWs as presented in Figure S9. Therefore, in this work CdSe/CdZnS

© 2025 The Author(s). Advanced Optical Materials published by Wiley-VCH GmbH

21951071, 2026, 12, Downloaded from https://advanced.onlinelibrary.wiley.com/doi/10.1002/adom.202502254 by Hilmi Demir - Bilkent University , Wiley Online Library on [29/03/2026]. See the Terms and Conditions (https://onlinelibrary.wiley.com/terms-and-conditions) on Wiley Online Library for rules of use; OA articles are governed by the applicable Creative Commons License

CQWs were used as emitters rather than CdSe/ZnS core/shell CQWs.

The OA and OLA ligands of the core/shell CQWs possess long organic chains, which limits the charge transport rate and the spin-injection efficiency in spin-LEDs by enlarging the electron-hopping distance and creating a potential barrier.[10,33,34] To enhance the spin-injection efficiency in the spin-LEDs, we exchanged the long chain OA ($C_{18}H_{34}O_2$) and OLA ($C_{18}H_{35}NH_2$) ligands with shorter chain 2-ethylhexane-1-thiol (EHT), $C_8H_{18}S$. The EHT is expected to increase the charge transport rate and spin-injection efficiency by shortening the distance between the spin-injecting Fe_3O_4 layer and the active electroluminescent layer.[10,33,34] The PL and absorption spectra of the CQWs remained unchanged after the ligand exchange, as can be seen in Figure 1c. In addition, the PLQY dropped slightly to 85% after the ligand exchange, which proves the robust and efficient attachment of EHT ligands to the CQWs. To confirm the ligand-exchange, we performed the Fourier-transform infrared spectroscopy (FTIR) on the CQWs as presented in Figure 1d. The vanishing of the peak at 1641 cm^{-1}, which is associated with the vibration mode of the amine group of OLA, signifies the successful ligand exchange with EHT.

The obtained CdSe/CdZnS core/shell CQWs passivated with EHT and emitting at 630 nm were employed in the spin-LED structure as the active emissive layer. The fabricated spin-LED structure includes an indium tin oxide (ITO) anode electrode on a glass substrate, a hole injection layer of poly(ethylenedioxythiophene)-polystyrenesulfonate (PEDOT:PSS), a hole transport layer of poly(N,N9-bis(4-butylphenyl)-N,N9-bis-(phenyl)-benzidine) (poly-TPD), a CdSe/CdZnS core/shell CQWs emissive layer, a Fe_3O_4 spin-injection layer, a ZnO electron transport layer, and an aluminum cathode electrode. The Fe_3O_4 layer is designed to be at the electron side of the device to inject spin-polarized electrons. Additionally, we fabricated a control device without an Fe_3O_4 layer to investigate potential spurious effects, which we named as the non-magnetic LED. The schematic of the spin-LED showing each layer and the corresponding energy band diagram is presented in **Figure 2**a,b, respectively. Energy band diagrams of Al, ZnO, CQWs, p-TPD, PEDOT:PSS, and ITO were obtained from previous works on solution-processed LEDs with similar device architecture,[34,35] while that of Fe_3O_4 was obtained from a previous report on thin films.[36] In this device, PEDOT:PSS and poly-TPD were consecutively spin-coated on ITO patterned glass substrate. A monolayer of face-down oriented CdSe/CdZnS core/shell CQWs was deposited using a self-assembly technique, which was previously developed by our group.[34,37] Then Fe_3O_4 and ZnO layers were spin-coated consecutively, before the evaporation of an Al cathode layer. In this device structure, the electron–hole pair is confined in the CdSe/CdZnS core/shell CQWs emissive layer since the PEDOT:PSS layer transports the holes and blocks the electrons, while the ZnO layer allows the transport of electrons and blocks the holes.

The cross-sectional TEM image of the fabricated spin-LED, showing each deposited layer, is presented in Figure 2c. All of the deposited layers, which can be clearly seen in the cross-sectional image, appear to be smooth and uniform according to the cross-sectional image. According to the cross-sectional TEM image, the thickness of the Fe_3O_4 layer is 55 nm, which corresponds to a thickness of 5 monolayers of Fe_3O_4. On the other hand, the thickness of the CQW layer is ≈5 nm, close to the thickness of our CQWs, which suggests the successful deposition of a monolayer of face-down oriented CQWs on the Fe_3O_4 layer. In the closed-view cross-sectional image (left panel of Figure 2c), a monolayer of CQWs lying in face-down orientation can be seen clearly, which clearly demonstrates successful utilization of the self-assembly technique in our spin-LED structure. Such a monolayer of CQWs is crucial to minimize the polarization losses due to the hopping of the electrons between the CQWs. The top-view scanning electron microscopy (SEM) image shows a close-packed, self-assembled monolayer of CQWs on a substrate coated with the layers of ITO/PEDOT:PSS/p-TPD (Figure 2d). The roughness of the face-down CQW and Fe_3O_4 layer on the CQW layer on a substrate coated with the layers of ITO/PEDOT:PSS/p-TPD was measured through atomic force microscopy (AFM), as presented in Figure 2e. According to the AFM scan results, the CQW layer and the Fe_3O_4 layer on the CQW layer have a roughness of 1.8 and 2.0 nm, respectively.

Our spin-LED exhibits a narrow EL emission at 626 nm with a FWHM of 31 nm at $T = 3$ K and zero magnetic field as given in Figure 2f. The EL spectrum is very similar to the PL spectra from similar CQWs,[38–41] which confirms that the EL emission originates from the excitonic emission of the core/shell CQWs as depicted in **Figure 3**a. The EL emission profile spectrally remains the same as the voltage was increased up to 7 V as a result of strong confinement of the charge carriers in the CQW active layer, as presented in Figure S2 (Supporting Information). The turn-on voltage of the device drops as temperature increases from 2.5 to 290 K which can be attributed to an increase in the conductivity of the organic layers as presented in Figure S3.

In Figure 3a, the schematic of carrier recombination process under an applied magnetic field in our spin-LED is provided. In this device the Fe_3O_4 layer drives the injection of spin polarized electrons as depicted. The left circularly polarized (σ_+) and right circularly polarized (σ_-) EL spectra from the spin-LED at $T = 3$ K and a magnetic field $B = 5$ T in the direction of light propagation normal to the device layers are shown in Figure 3b. The red line indicates the σ_+ component of the EL spectrum, while the black line indicates the σ- component. The blue line represents the circular polarization P determined using the relation $P = \frac{I_+ - I_-}{I_+ + I_-}$, where $I_+(I_-)$ is the intensity of the $\sigma_+(\sigma_-)$ EL component, respectively. In our CQWs, only the heavy hole band is responsible for the recombination process, which means circular polarization is equal to the electron spin polarization.[4] The σ_+ (σ_-) EL arises due to radiative recombination processes between spin $-\frac{1}{2}$ ($+\frac{1}{2}$) electrons and spin $+\frac{3}{2}$ ($-\frac{3}{2}$) holes. It can be seen that at a field of 5 T, the intensities of the σ_+ and σ_- are different, resulting in $P = 4.5\%$ at the peak wavelength of 630 nm (blue line). This indicates that the majority of the recombining electrons, which are injected through the magnetic Fe_3O_4 layer, are in the $-\frac{1}{2}$ spin state. In Figure S4 (Supporting Information), we show the EL spectra at $B = -5$ T with a resulting P value of –4.5%. The magnetic field dependence of the EL circular polarization was measured by using field sweeps from 5 to -5 T, and at each field value P was measured. The plot of the EL circular polarization P versus B for the above process is depicted in Figure 3c. In addition, from the P versus B plot of Figure 3e, we determined that the

© 2025 The Author(s). Advanced Optical Materials published by Wiley-VCH GmbH

21951071, 2026, 12, Downloaded from https://advanced.onlinelibrary.wiley.com/doi/10.1002/adom.202502254 by Hilmi Demir - Bilkent University , Wiley Online Library on [29/03/2026]. See the Terms and Conditions (https://onlinelibrary.wiley.com/terms-and-conditions) on Wiley Online Library for rules of use; OA articles are governed by the applicable Creative Commons License

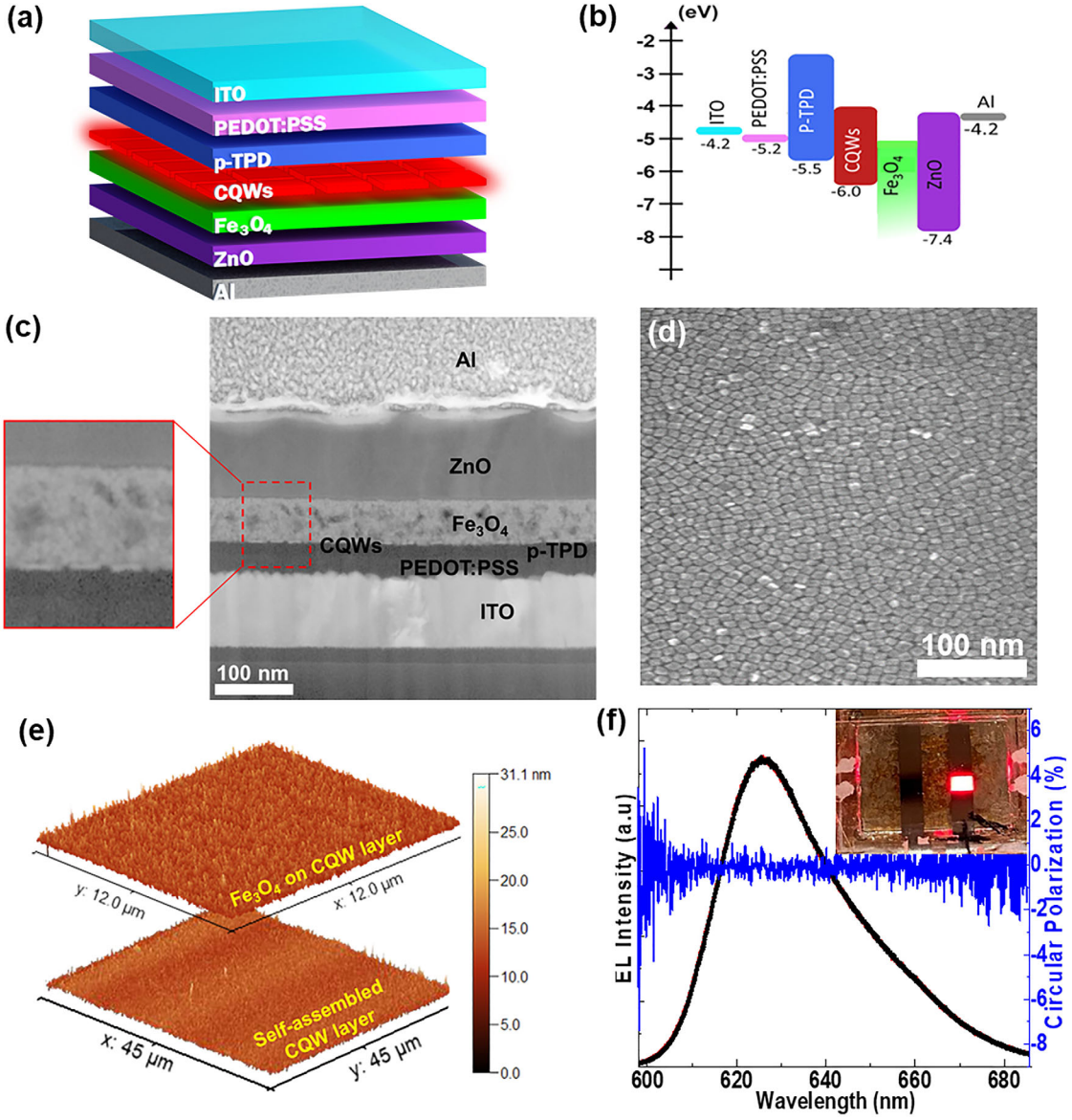

Figure 2. Structural characterizations of the fabricated spin-LED. a) Schematic of the device architecture. b) Energy band diagram of the LED structure. c) A cross-sectional TEM image of the LED. d) SEM image of the all-face-down self-assembled monolayer of CQWs on a substrate coated with the layers of ITO/PEDOT:PSS/p-TPD. e) AFM scan results of face-down CQW layer and Fe_3O_4 layer on CQW layer on a substrate coated with the layers of ITO/PEDOT:PSS/p-TPD. f) EL spectra of our LED device operating at 10 V, 0 T, and 3 K. The inset of (f) shows a photograph of the working device.

average remanent polarization P_{rem}≈1% and the average coercive field B_c≈0.16 T. Such hysteretic polarization clearly signifies spin injection from the ferrimagnetic Fe_3O_4 nanoparticles. The magnetization hysteresis curves of Fe_3O_4 at 5 and 290 K are provided in Figure 3f. The EL circular polarization shown in Figure 3c,e mimics the magnetization curve given in Figure 3f.

Figure 3b,c,e clearly shows that the spin polarization of the injected electrons responsible for the EL circular polarization is due to the presence of the Fe_3O_4 nanoparticles. This is further confirmed by the plot of P versus B from the non-magnetic LED shown in Figure S5 (Supporting Information). The plot of P versus B for the non-magnetic LED exhibits a linear relationship with a negative slope at all field values. The negative slope of the circular polarization is due to the lifted spin degeneracy under the applied field as a result of Zeeman splitting and the thermalization of carriers to the lowest state.[38] Further evidence that the injection of spin-polarized electrons is due to the presence of the ferromagnetic Fe_3O_4 nanoparticle layer in spin-LED is provided by the temperature evolution of the P versus B plot for the spin-LED shown in Figure 3d. As the device temperature is increased from 3 to 55 K the saturation value of P decreases to 1 % and at T = 100 K it vanishes. Recently, the spin-LEDs based on chiral molecules were shown to exhibit circularly polarized emission at room-temperature. However, these spin-LEDs based on chiral molecules do not have polarization modulation capability and their circular polarization is usually quite low < 1%.[11,42,43]

© 2025 The Author(s). Advanced Optical Materials published by Wiley-VCH GmbH

21951071, 2026, 12, Downloaded from https://advanced.onlinelibrary.wiley.com/doi/10.1002/adom.202502254 by Hilmi Demir - Bilkent University , Wiley Online Library on [29/03/2026]. See the Terms and Conditions (https://onlinelibrary.wiley.com/terms-and-conditions) on Wiley Online Library for rules of use; OA articles are governed by the applicable Creative Commons License

21951071, 2026, 12, Downloaded from https://advanced.onlinelibrary.wiley.com/doi/10.1002/adom.202502254 by Hilmi Demir - Bilkent University , Wiley Online Library on [29/03/2026]. See the Terms and Conditions (https://onlinelibrary.wiley.com/terms-and-conditions) on Wiley Online Library for rules of use; OA articles are governed by the applicable Creative Commons License

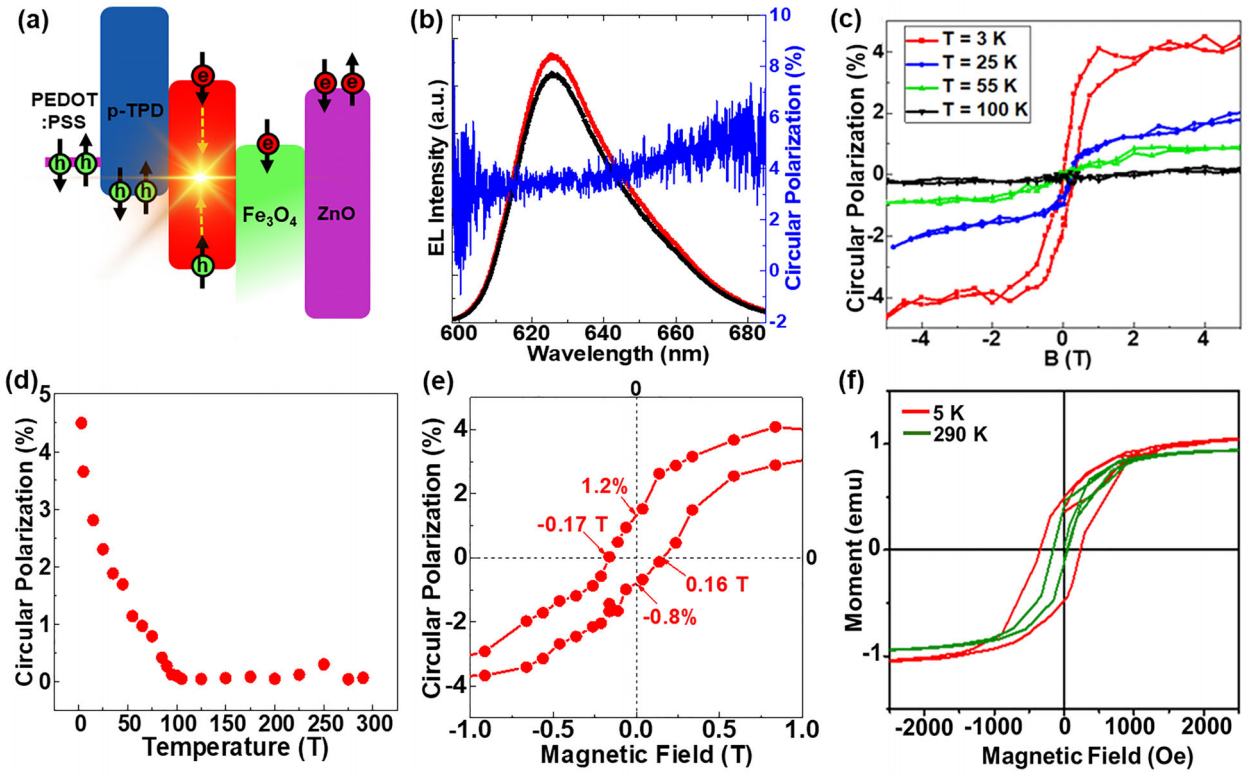

Figure 3. Magneto-optical measurements demonstrating spin-polarized emission from a Fe_3O_4-based spin-LED. a) The schematic of the carrier recombination process in the device. b) EL spectra of left-circularly polarized (red line) and right-circularly polarized light (black line) from our LED device operating at 10 V, 5 T, and 3 K. c) Circular polarization of EL at various temperatures and applied magnetic fields. d) Circular polarization of EL (at 5 T) as a function of the temperature. e) Coercivity of circular polarization of EL at 3K. f) Magnetization of Fe_3O_4 nanoparticles as a function of the applied magnetic field at 5 and 290 K.

In a spin-LED, the carriers are electrically injected into the active layer from a magnetic layer with a net spin polarization. To investigate the spin injection efficiency in the spin-LED, we measured the spin relaxation lifetime with the transient absorption and recombination lifetime measurements with TRPL. The details of the measurements and the setups are given in the Supporting Information. The measurements were performed from 3 K to room-temperature. The degree of circular polarization in a spin-LED is dependent on spin injection efficiency, spin-relaxation lifetime and recombination lifetime according to a rate equation model:[3,4,6,11]

$$P = \frac{\Pi}{1 + \frac{\tau_r}{\tau_S}} \quad (1)$$

where Π is the spin injection efficiency, τs is the spin relaxation lifetime, and τr is the recombination lifetime. By determining P, τs and τr independently, Π can be obtained.[11]

We measured the temperature-dependent spin relaxation lifetimes with spin-polarized transient absorption spectroscopy.[32] Transient absorption experiments were performed using a titanium:sapphire laser with a 35 fs pulse width and a 2 kHz repetition rate at low fluences (corresponding to 1>> excitons per CQW). The wavelength of the pump was set near to the band-edge transition (≈10 nm blue side of the band-edge transition) to retain spin polarization and avoid appreciable hot carrier relaxation. To deduce the spin-polarized information from the TA maps, the co-polarized TA data (meaning both pump and probe have the same circular polarization) were subtracted from separately measured cross-polarized data (meaning pump and probe have the orthogonal circular polarization).[32] The dynamic behavior of the spin-selective photoinduced absorption (PIA) feature of CdSe/CdZnS core/shell samples from 3 to 295 K is provided in Figure S7 (Supporting Information) together with decay dynamics fittings.

The obtained intensity-averaged lifetimes at various temperatures are provided in **Figure** 4a. As can be seen in Figure 4a, the spin relaxation lifetimes shorten as the temperature is raised. This trend is almost identical with the temperature dependence of the circular polarization from the EL. This indicates that the vanishing circular polarization at high temperatures is caused by the shortening of the spin relaxation lifetimes. The spin relaxation lifetime depends almost linearly on $T^{-0.5}$ as presented in Figure S8 (Supporting Information), which suggests that D'yakanov–Perel spin relaxation mechanism, which was known to dominate at higher temperatures and in medium gap materials,[10,44,45] is responsible for such temperature-dependent spin relaxation lifetimes, as previously reported in QWs grown by epitaxial techniques.[46]

In addition, we performed temperature-dependent TRPL to obtain the recombination lifetimes. We studied the PL lifetime in the device from 3 K to room-temperature and the

© 2025 The Author(s). Advanced Optical Materials published by Wiley-VCH GmbH

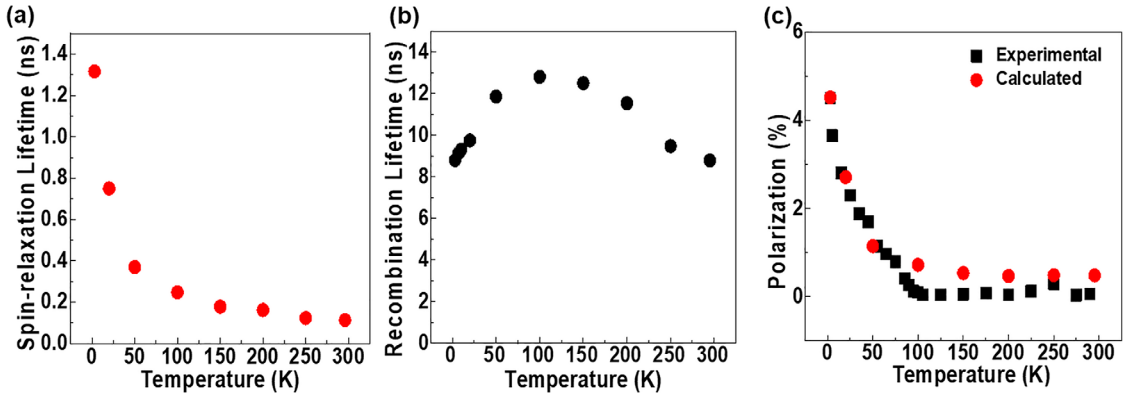

Figure 4. Polarization dynamics of the spin-LED. a) Temperature dependence of spin-relaxation lifetimes obtained by spin-polarized transient absorption spectroscopy. b) Temperature dependence of recombination lifetimes obtained by time-resolved photoluminescence spectroscopy. c) Temperature dependence of polarization values obtained by magneto-EL spectroscopy and rate equation model using a spin injection efficiency value of 35%, along with the spin-relaxation lifetimes provided in (a) and the recombination lifetimes given in (b).

intensity-averaged lifetimes are provided in Figure 4b. The TRPL decay curves with the fittings are provided in Figure S10 (Supporting Information). We found that the recombination lifetime of the exciton in the CQW layer is ≈9 ns at 3 K in our spin-LED structure, whereas the spin relaxation lifetime is ≈1.3 ns at 3 K. Using Equation (1), the spin-injection efficiency of our device is calculated to be ≈35%. This value is about ½ of the carrier spin polarization of 70% previously reported in Fe_3O_4 nanoparticles,[27] and is similar to spin injection efficiencies from Fe Schottky contacts to GaAs QWs.[4] The spin injection efficiency is lower (19%) in the spin-LED fabricated with CQWs passivated with long-chain OA and OLA ligands as can be seen from Figure S6 (Supporting Information), showing lower polarization values compared to the spin-LED having CQWs passivated with short-chain EHT.

This spin efficiency is expected to be insensitive to temperature since the tunneling process is independent of temperature.[4,47] The lower spin-injection efficiency can be attributed to the passivation of Fe_3O_4 nanoparticles with longer chain ligands enhancing the spin scattering during the carrier hopping from Fe_3O_4 nanoparticles to CQWs.[10] Hence, changing the long OA and OLA ligands presents an effective pathway for enhancing the P of the EL emission by improving the tunneling between interfacial layers.[10]

As we know the spin injection efficiency, which is expected to be temperature independent, one can calculate the P values at different temperatures based on Equation (1), using the measured spin-relaxation and recombination lifetimes at various temperatures. As shown in Figure 4c, the measured value of P (P_{exp}) (black dots) and the calculated P (P_{cal}) (red dots) closely match with each other. From this result, it appears that the main limiting factor for the P value in the EL appears to be the relatively short spin-relaxation lifetime as compared to the recombination lifetime, which is similar to spin-LEDs based on $CsPbI_3$ perovskites.[11] In addition, the rapid decrease in τs with increasing temperature is responsible for the reduction in P value with temperature. To improve the EL circular polarization and realize room-temperature spin-LEDs, the recombination times can be made one or two orders of magnitude shorter via Purcell effect by employing an additional plasmonic silver or gold layer between the CQW layer and the hole transport layer in the device structure.[48,49]

3. Conclusion

In summary, we have demonstrated the first all-solution-processed spin-LEDs using electrical spin injection into colloidal QWs from magnetic nanoparticles, which leads to circularly polarized EL emission modulated by an external magnetic field. This solution-processed spin-LED yields a circular polarization up to 4.5% at 3 K, with a net circular polarization that persists up to 100 K in the absence of a magnetic field, due to the remnant magnetization of the Fe_3O_4 nanoparticles. The calculated spin-injection efficiency of 35% is lower than the carrier spin polarization of the injector, which can be attributed to the longer ligands of the Fe_3O_4 nanoparticles. Such an effect can be resolved by exchanging the long ligands (OA and OLA) of Fe_3O_4 with shorter ligands. In addition, we elucidated the spin relaxation mechanism in CQWs using temperature-dependent polarized pump-probe measurements, which highlight the D'yakanov–Perel mechanism as the driver of the observed temperature-dependent spin relaxation lifetimes.

This newly developed, all-solution-processed spin-LED structure having magnetic nanoparticles as a spin polarizer layer, is expected to open unprecedented routes for future advanced opto-spintronic devices based on nanocrystals which have shorter recombination and long spin-relaxation lifetimes, and magnetic nanoparticles with custom-designed magnetic and electronic properties, thanks to the significant advancements in the colloidal synthesis methods. In addition, recombination lifetimes can be shortened considerably (≈two orders of magnitude) via Purcell effect enhancement of the radiative recombination rate by employing an additional plasmonic layer in the spin-LEDs to achieve spin-LEDs operating at room-temperature efficiently. With the ability to control optical polarization, these results based on solution-processed spintronics together with further improvements in the ligands and Purcell effect through the usage of plasmonic particles are very encouraging for the realization of room-temperature advanced spintronic devices for applications in optical switches, modulators, and cryptography.

© 2025 The Author(s). Advanced Optical Materials published by Wiley-VCH GmbH

21951071, 2026, 12, Downloaded from https://advanced.onlinelibrary.wiley.com/doi/10.1002/adom.202502254 by Hilmi Demir - Bilkent University , Wiley Online Library on [29/03/2026]. See the Terms and Conditions (https://onlinelibrary.wiley.com/terms-and-conditions) on Wiley Online Library for rules of use; OA articles are governed by the applicable Creative Commons License

4. Experimental Section

Synthesis of Fe_3O_4 Magnetic Nanoparticles: The synthesis of Fe_3O_4 magnetic nanoparticles was carried out using a previously reported recipe.[16] Iron(III) acetylacetonate (2 mmol), 1,2-hexadecanediol (10 mmol), OA (6 mmol), OLA (6 mmol), and benzyl ether (12 mL) were mixed and stirred vigorously in a three-neck flask for 20 min under a flow of nitrogen at room-temperature. The mixture was heated to 200 °C and kept there for 2 h. Then, the solution was heated to ≈300 °C and kept there for 2 h. Finally, the reaction was cooled down to room-temperature and Fe_3O_4 magnetic nanoparticles were isolated from the side products with selective precipitation using hexane as a solvent and acetone as an anti-solvent. Hexane and acetone was added to the solution, and then the mixture was centrifuged at 6000 rpm for 6 min. The supernatant was discarded, and the black precipitate was redispersed in 5 mL of hexane for further use.

Synthesis of CdSe/CdZnS Core/Shell Colloidal Quantum Wells (CQWs): First, seed CdSe CQWs were synthesized. The synthesis of seed CQWs was carried out using a previously reported recipe.[50] 13 mg of Se, 170 mg of cadmium myristate, and 15 mL of ODE were put into a flask and degassed for 30 min at room-temperature. Then, under a nitrogen flow, the temperature was set to 240 °C, and 50 mg of cadmium acetate dihydrate was added when the temperature reached 200 °C. 1 mL of oleic acid was added 1 min after reaching the 240 °C to stop the synthesis. Then, the mixture containing the CQWs was cooled down to room-temperature. To remove the unreacted species and side products, selective precipitation was performed using hexane and ethanol. The obtained CdSe CQWs were stored in hexane for further use.

The synthesis of core/shell CQWs was carried out using a previously reported recipe.[34] 22.5 mg of anhydrous cadmium acetate ($Cd(OAc)_2$), 55 mg of anhydrous zinc acetate ($Zn(OAc)_2$), 1 mL of OA, 7.5 mL of octadecene (ODE), and 1 mL of 4 monolayer CdSe CQWs in hexane with an optical density of 120 (at 350 nm) were loaded into a three-neck flask. This mixture was degassed under vacuum, first at room-temperature for 1 h and then at 80 °C for 30 min, to remove hexane, air, and other volatile species from the reaction medium. The atmosphere was then switched to nitrogen, 2 mL of oleylamine was swiftly injected into the flask, and the temperature was set to 220 °C. As the temperature reached to160 °C, injecting a mixture of 280 µL of octanethiol, and 16 mL of ODE was begun at a rate of 20 mL h^{-1} using a syringe pump, and the temperature was set to 295 °C. Once the temperature reached 240 °C, the injection rate was reduced to 4 mL h^{-1}. The reaction was stopped by removing the heating mantle and ceasing injection once 5 mL of the octanethiol-ODE mixture had been injected, at which point the emission wavelength had reached 640 nm. To remove unreacted species and side products, selective precipitation was performed using hexane and ethanol. First, 10 mL of hexane were added to the reaction mixture at room-temperature and centrifuged at 6000 rpm for 6 min. The precipitate was discarded, and 6–7 mL of ethanol was added to the supernatant, which was centrifuged at 6000 rpm for 6 min. The supernatant was discarded, and precipitate was redispersed in 5 mL of hexane to store.

Synthesis of ZnO Nanoparticles: 3 mmol zinc acetate dihydrate was dissolved in 30 mL of dimethyl sulfoxide (DMSO) solution and stirred vigorously at 1000 rpm. Then, a mixture of 5.5 mmol tetramethylammonium hydroxide (TMAH) in 10 mL ethanol was injected into the Zn-acetate solution at a rate of 40 mL h^{-1} under ambient conditions. Then, the mixture was kept stirring for 2 h. Afterward, ZnO nanoparticles were precipitated by adding ethyl acetate and redispersed in ethanol. To improve the solubility of ZnO nanoparticles, 160 µL of ethanolamine was added to the mixture and kept stirring for 2 h inside the nitrogen filled glovebox. Finally, the resulting nanoparticles were washed by addition of ethyl acetate and redispersed in ethanol.

Details of Device Fabrication and Characterization: The fabrication process began by cleaning pre-patterned ITO-coated substrates in four stages: detergent, distilled water, acetone, and isopropanol, each for 15 min. A PEDOT:PSS/isopropanol (1:1) solution (Osilla Al 4083, filtered through a 0.25 µm PTFE membrane) was then spin-coated onto the cleaned ITO-coated glass substrates at 4000 rpm for 60 min. The coated substrates were baked at 120 °C for 30 min. Afterward, the substrates were transferred to a nitrogen-filled glove box (with O_2 and H_2O levels kept below 0.1 ppm). Inside the glove box, the substrates were further baked for 5 min at 110 °C to remove any residual moisture absorbed during the transfer. Then, poly-TPD (8 mg mL^{-1} in chlorobenzene) was deposited by spin-coating. Self-assembly method was used for deposition of a single-layer CQWs by following a previously reported work from the group.[2] After that, Fe_3O_4 (10 mg mL^{-1} in hexane), and ZnO (25 mg/mL in ethanol) layers were sequentially deposited by spin-coating. The spin-coating was performed at 2000 rpm for 1 min per layer. The poly-TPD layer was baked at 110 °C for 30 min, while the CQWs, Fe_3O_4, and ZnO layers were baked at 60 °C for 20 min each. Finally, a 100 nm aluminum layer was deposited through a shadow mask using an oxygen-free thermal evaporation system, creating a 4.5 mm^2 active area. The devices were then encapsulated using a sapphire coverslip and UV-curable resin.

For electrical characterization, an Agilent Technologies (U3606A) electrometer was used to measure current–voltage characteristics. Atomic force microscopy (AFM) analysis was carried out using a PSIA Training instrument, and microstructure analysis was conducted with an FEI FIB/SEM system. Transmission electron microscopy (TEM) images were acquired using an FEI (TECNAI) instrument.

Details of Magneto-Electroluminescence (MEL) Measurements: The top of the fabricated spin-LEDs was covered with a sapphire piece right after fabrication to protect the layers during the MEL measurements and because of the good heat conductivity of the sapphire. The LEDs were placed in a variable temperature 7 tesla optical closed cycle magnet cryostat after creating contacts with silver paste and Cu wires. The temperature can be varied from 2 to 400 K with temperature stability of ≈± 10 mK at each temperature setting. Photos of a spin-LED after creating contacts with Cu wires, after mounting sample to the sample holder, and after lit up are shown in Figure S11 (Supporting Information).

The emitted EL was collected and focused onto the entrance slit of a single monochromator equipped with a cooled CCD multichannel detector. A combination of quarter-wave plate and a linear polarizer placed immediately before the entrance slit was used to separate the two circularly polarized components of each EL spectrum.

Details of Temperature-Dependent Time-Resolved Photoluminescence Measurements: A custom-built micro-photoluminescence (µ-PL) setup was utilized for conducting temperature-dependent time-resolved photoluminescence (TRPL) measurements. The sample was mounted on an XYZ positioner in a closed-cycle cryostat (Attodry 1000) with a base temperature of 3 K. The sample was excited using a 532 nm picosecond pulsed laser diode operating under pulse mode at 5 MHz repetition rate, and the emitted PL light was collected through a low-temperature compatible microscope objective with a numerical aperture (NA) of 0.82 and directed through a 550 nm long-pass filter (Thorlabs FEL0550) before reaching the detector. After passing through the filter, the light was directed to a single-photon avalanche diode (SPAD) with a photon timing resolution of 50 ps. The HydraHarp 400 multichannel picosecond event timer and TCSPC module (PicoQuant) were used to record PL decay curves. Temperature-dependent measurements were conducted by progressively increasing the temperature from 3 K to 295 K via a temperature controller (Lake Shore Model 335).

Supporting Information

Supporting Information is available from the Wiley Online Library or from the author.

Acknowledgements

The authors gratefully acknowledge the financial support in part from the Singapore Agency for Science, Technology and Research (A*STAR) MTC program under grant number M21J9b0085, Ministry of Education, Singapore, under its Academic Research Fund Tier 1 (MOE-RG62/20), and in part from TUBITAK 121C266 and 20AG001. H.V.D. also acknowledges

© 2025 The Author(s). Advanced Optical Materials published by Wiley-VCH GmbH

21951071, 2026, 12, Downloaded from https://advanced.onlinelibrary.wiley.com/doi/10.1002/adom.202502254 by Hilmi Demir - Bilkent University , Wiley Online Library on [29/03/2026]. See the Terms and Conditions (https://onlinelibrary.wiley.com/terms-and-conditions) on Wiley Online Library for rules of use; OA articles are governed by the applicable Creative Commons License

support from TUBA-Turkish Academy of Sciences and TUBITAK 2247-A National Leader Researchers Program (121C266). B.C. acknowledges support from TUBITAK 124F030 and TUBITAK 2218 National Postdoctoral Research Fellowship Program (120C219). H.Z. acknowledges support from US NSF ECCS-2042085 and NSF DMR-2242796. Work performed at the Center for Nanoscale Materials, a U.S. Department of Energy Office of Science User Facility, was supported by the U.S. DOE, Office of Basic Energy Sciences, under Contract No. DE-AC02-06CH11357. I.S acknowledges funding from TUBITAK under (Grant No. 122F389).

Conflict of Interest

The authors declare no conflict of interest.

Author Contributions

S.D., A.B. and B.C. contributed equally to this work. The manuscript was written through the contributions of all authors. All authors have given approval to the final version of the manuscript.

Data Availability Statement

The data that support the findings of this study are available from the corresponding author upon reasonable request.

Keywords

circularly polarized electroluminescence, colloidal magnetic nanoparticles, colloidal quantum wells, solution-processed LEDs, spin-light emitting diodes

Received: July 18, 2025
Revised: November 12, 2025
Published online: December 18, 2025

[1] I. Žutić, J. Fabian, D. Sarma, S. Spintronics, *Rev. Mod. Phys.* **2004**, *76*, 323.
[2] A. Hirohata, K. Yamada, Y. Nakatani, I. L. Prejbeanu, B. Diény, P. Pirro, B. Hillebrands, *J. Magn. Magn. Mater.* **2020**, *509*, 166711.
[3] B. T. Jonker, G. Kioseoglou, A. T. Hanbicki, C. H. Li, P. E. Thompson, *Nat. Phys.* **2007**, *3*, 542.
[4] B. T. Jonker, *Proc. IEEE* **2003**, *91*, 727.
[5] R. Fiederling, M. Keim, G. Reuscher, W. Ossau, G. Schmidt, A. Waag, L. W. Molenkamp, *Nature* **1999**, *402*, 787.
[6] G. Kioseoglou, A. Petrou, *J. Low Temp. Phys.* **2012**, *169*, 324.
[7] A. Hirohata, K. Takanashi, *J. Phys. D: Appl. Phys.* **2014**, *47*, 193001.
[8] S. Kak, P. Verma, G. MacDonald, in *The Nature of Light: What are Photons? IV*, SPIE, San Diego, California **2011**, *8121*.
[9] D. D. Awschalom, J. Warnock, *Phys. Rev. Lett.* **1987**, *58*, 812.
[10] M. Holub, P. Bhattacharya, *J. Phys. D: Appl. Phys.* **2007**, *40*, R179.
[11] Y. H. Kim, Y. Zhai, H. Lu, X. Pan, C. Xiao, E. A. Gaulding, S. P. Harvey, J. J. Berry, Z. V. Vardeny, J. M. Luther, M. C. Beard, *Science* **2021**, *371*, 1129.
[12] C. Adelmann, X. Lou, J. Strand, C. J. Palmstrøm, P. A. Crowell, *Phys. Rev. B* **2005**, *71*, 121301.
[13] A. T. Hanbicki, B. T. Jonker, G. Itskos, G. Kioseoglou, A. Petrou, *Appl. Phys. Lett.* **2002**, *80*, 1240.
[14] B. T. Jonker, Y. D. Park, B. R. Bennett, H. D. Cheong, G. Kioseoglou, A. Petrou, *Phys. Rev. B* **2000**, *62*, 8180.
[15] Y. Ohno, D. K. Young, B. Beschoten, F. Matsukura, H. Ohno, D. D. Awschalom, *Nature* **1999**, *402*, 790.
[16] S. Sun, H. Zeng, *J. Am. Chem. Soc.* **2002**, *124*, 8204.
[17] S. Sun, H. Zeng, D. B. Robinson, S. Raoux, P. M. Rice, S. X. Wang, G. Li, *J. Am. Chem. Soc.* **2004**, *126*, 273.
[18] H. Zeng, P. M. Rice, S. X. Wang, S. Sun, *J. Am. Chem. Soc.* **2004**, *126*, 11458.
[19] H. Yu, M. Chen, P. M. Rice, S. X. Wang, R. L. White, S. Sun, *Nano Lett.* **2005**, *5*, 379.
[20] W. Shi, H. Zeng, Y. Sahoo, T. Y. Ohulchanskyy, Y. Ding, Z. L. Wang, M. Swihart, P. N. Prasad, *Nano Lett.* **2006**, *6*, 875.
[21] S. Sun, C. B. Murray, D. Weller, L. Folks, A. Moser, *Science* **2000**, *287*, 1989.
[22] H. Zeng, J. Li, J. P. Liu, Z. L. Wang, S. Sun, *Nature* **2002**, *420*, 395.
[23] H. Huang, S. Delikanli, H. Zeng, D. M. Ferkey, A. Pralle, *Nat. Nanotechnol.* **2010**, *5*, 602.
[24] X. Yin, S. E. Russek, G. Zabow, F. Sun, J. Mohapatra, K. E. Keenan, M. A. Boss, H. Zeng, J. P. Liu, A. Viert, S. H. Liou, J. Moreland, *Sci. Rep.* **2018**, *8*, 11863.
[25] S. He, H. Zhang, Y. Liu, F. Sun, X. Yu, X. Li, L. Zhang, L. Wang, K. Mao, G. Wang, Y. Lin, Z. Han, R. Sabirianov, H. Zeng, *Small* **2018**, *14*, 1800135.
[26] X. Yu, S. Gao, D. Wu, Z. Li, Y. Mi, T. Yang, F. Sun, L. Wang, R. Liu, S. He, Q. Ge, Y. Lv, A. Xu, H. Zeng, *Small* **2022**, *18*, 2104626.
[27] H. Zeng, C. T. Black, R. L. Sandstrom, P. M. Rice, C. B. Murray, S. Sun, *Phys. Rev. B* **2006**, *73*, 020402.
[28] M. Furis, J. A. Hollingsworth, V. I. Klimov, S. A. Crooker, *J. Phys. Chem. B* **2005**, *109*, 15332.
[29] S. Ithurria, M. D. Tessier, B. Mahler, R. P. S. M. Lobo, B. Dubertret, A. L. Efros, *Nat. Mater.* **2011**, *10*, 936.
[30] S. Shendre, S. Delikanli, M. Li, D. Dede, Z. Pan, S. T. Ha, Y. H. Fu, P. L. Hernández-Martínez, J. Yu, O. Erdem, A. I. Kuznetsov, C. Dang, T. C. Sum, H. V. Demir, *Nanoscale* **2019**, *11*, 301.
[31] Y. Altintas, U. Quliyeva, K. Gungor, O. Erdem, Y. Kelestemur, E. Mutlugun, M. V. Kovalenko, H. V. Demir, *Small* **2019**, *15*, 1804854.
[32] P. I. Martin, S. Panuganti, J. C. Portner, N. E. Watkins, M. G. Kanatzidis, D. V. Talapin, R. D. Schaller, *Nano Lett.* **2023**, *23*, 1467.
[33] D. K. Young, E. Johnston-Halperin, D. D. Awschalom, Y. Ohno, H. Ohno, *Appl. Phys. Lett.* **2002**, *80*, 1598.
[34] H. D. Baruj, I. Bozkaya, B. Canimkurbey, A. T. Isik, F. Shabani, S. Delikanli, S. Shendre, O. Erdem, F. Isik, H. V. Demir, *Small* **2023**, *19*, 2206582.
[35] F. Shabani, H. Dehghanpour Baruj, I. Yurdakul, S. Delikanli, N. Gheshlaghi, F. Isik, B. Liu, Y. Altintas, B. Canımkurbey, H. V. Demir, *Small* **2022**, *18*, 2106115.
[36] M. Fonin, R. Pentcheva, Y. S. Dedkov, M. Sperlich, D. V. Vyalikh, M. Scheffler, U. Rüdiger, G. Güntherodt, *Phys. Rev. B* **2005**, *72*, 104436.
[37] O. Erdem, K. Gungor, B. Guzelturk, I. Tanriover, M. Sak, M. Olutas, D. Dede, Y. Kelestemur, H. V. Demir, *Nano Lett.* **2019**, *19*, 4297.
[38] S. Delikanli, M. Z. Akgul, J. R. Murphy, B. Barman, Y. Tsai, T. Scrace, P. Zhang, B. Bozok, P. L. Hernández-Martínez, J. Christodoulides, A. N. Cartwright, A. Petrou, H. V. Demir, *ACS Nano* **2015**, *9*, 12473.
[39] E. V. Shornikova, D. R. Yakovlev, D. O. Tolmachev, V. Y. Ivanov, I. V. Kalitukha, V. F. Sapega, D. Kudlacik, Y. G. Kusrayev, A. A. Golovatenko, S. Shendre, S. Delikanli, H. V. Demir, M. Bayer, *ACS Nano* **2020**, *14*, 9032.
[40] A. Najafi, S. Tarasek, S. Delikanli, P. Zhang, T. Norden, S. Shendre, M. Sharma, A. Bhattacharya, N. Taghipour, J. Pientka, H. V. Demir, A. Petrou, T. Thomay, *ACS Appl. Nano Mater.* **2020**, *3*, 3151.
[41] D. O. Tolmachev, V. Y. Ivanov, D. R. Yakovlev, E. V. Shornikova, B. Witkowski, S. Shendre, F. Isik, S. Delikani, H. V. Demir, M. Bayer, *Nanoscale* **2020**, *12*, 21932.

© 2025 The Author(s). Advanced Optical Materials published by Wiley-VCH GmbH

21951071, 2026, 12, Downloaded from https://advanced.onlinelibrary.wiley.com/doi/10.1002/adom.202502254 by Hilmi Demir - Bilkent University , Wiley Online Library on [29/03/2026]. See the Terms and Conditions (https://onlinelibrary.wiley.com/terms-and-conditions) on Wiley Online Library for rules of use; OA articles are governed by the applicable Creative Commons License

[42] S. He, W. Lin, D. Yu, J. Shi, Z. Yin, C. Sun, H. Liu, C. Zhang, J. Yuan, S. Bai, S. Xiao, G. Long, M. Yuan, Y. Jiang, Y. Chen, Q. Song, *Nat. Commun.* **2025**, *16*, 2201.
[43] D. Chen, B. Tang, A. A. Sergeev, Y. Wu, H. Liu, D. Zhu, S. Hu, K. S. Wong, H. L. Yip, A. L. Rogach, *ACS Energy Lett.* **2025**, *10*, 815.
[44] C. H. Li, G. Kioseoglou, A. T. Hanbicki, R. Goswami, C. S. Hellberg, B. T. Jonker, M. Yasar, A. Petrou, *Appl. Phys. Lett.* **2007**, *91*, 262504.
[45] C. H. Li, G. Kioseoglou, O. M. J. van 't Erve, M. E. Ware, D. Gammon, R. M. Stroud, B. T. Jonker, R. Mallory, M. Yasar, A. Petrou, *Appl. Phys. Lett.* **2005**, *86*, 132503.
[46] F. Meier, B. P. Zakharchenya, *Optical Orientation*, Elsevier: North-Holland, Amsterdam, **1984**.
[47] E. Burstein, S. Lundqvist, *Tunneling Phenomena in Solids*, Springer, Boston, MA **1969**.
[48] S. V. Gaponenko, D. V. Guzatov, *Proc. IEEE* **2020**, *108*, 704.
[49] D. V. Guzatov, S. V. Gaponenko, H. V. Demir, *AIP Adv.* **2018**, *8*, 015324.
[50] M. D. Tessier, P. Spinicelli, D. Dupont, G. Patriarche, S. Ithurria, *Nano Lett.* **2014**, *14*, 207.

© 2025 The Author(s). Advanced Optical Materials published by Wiley-VCH GmbH

21951071, 2026, 12, Downloaded from https://advanced.onlinelibrary.wiley.com/doi/10.1002/adom.202502254 by Hilmi Demir - Bilkent University , Wiley Online Library on [29/03/2026]. See the Terms and Conditions (https://onlinelibrary.wiley.com/terms-and-conditions) on Wiley Online Library for rules of use; OA articles are governed by the applicable Creative Commons License